Effects of Cloud Heterogeneities on Shortwave Radiation: Comparison of Cloud-Top Variability and Internal Heterogeneity

TAMÁS VÁRNAI*

Department of Atmospheric and Oceanic Sciences, McGill University, Montreal, Quebec, Canada

ROGER DAVIES

Institute of Atmospheric Physics, University of Arizona, Tucson, Arizona

(Manuscript received 9 March 1998, in final form 28 October 1998)

ABSTRACT

This paper examines the processes through which cloud heterogeneities influence solar reflection. This question is important since present methods give numerical results only for the overall radiative effect of cloud heterogeneities but cannot determine the degree to which various mechanisms are responsible for it. This study establishes a theoretical framework that defines these mechanisms and also provides a procedure to calculate their magnitude. In deriving the framework, the authors introduce a one-dimensional radiative transfer approximation, called the tilted independent pixel approximation (TIPA). TIPA uses the horizontal distribution of slant optical thicknesses along the direct solar beam to describe the radiative influence of cloud heterogeneities when horizontal transport between neighbors is not considered. The effects for horizontal transport are then attributed to two basic mechanisms: trapping and escape of radiation, when it moves to thicker and thinner cloud elements, respectively.

Using the proposed framework, the study examines the shortwave radiative effects of cloud-top height and cloud volume extinction coefficient variations. It is shown and explained that identical variations in cloud optical thickness can cause much stronger heterogeneity effects if they are due to variations in geometrical cloud thickness rather than in volume extinction coefficient. The differences in albedo can exceed 0.05, and the relative differences in reflectance toward the zenith can be greater than 25% for overhead sun and 50% for oblique sun. The paper also explains a previously observed phenomenon: it shows that the trapping of upwelling radiation causes the zenith reflectance of heterogeneous clouds to increase with decreasing solar elevation.

1. Introduction

By simply observing a few typical clouds, one is immediately reminded that they seldom fit the ideal of the one-dimensional, homogeneous medium often assumed by simple radiative transfer theory. Clouds have surfaces that frequently are not smooth and defy simple analytic description. They may also have significant variability in the microphysical properties of their interiors. Clouds are inherently heterogeneous and require a three-dimensional viewpoint both in terms of their description and in order to understand their interaction with radiation.

Over the past several decades, the shortwave radiative effects of cloud heterogeneity have been the focus of numerous theoretical, and several observational, studies. The theoretical studies (e.g., Busygin et al. 1973; Davies 1978; and Marshak et al. 1995a) have indicated a wide variety of potential differences in behavior between horizontally homogeneous and heterogeneous clouds or cloud fields, some of which have been qualitatively confirmed by observation (e.g., Hayasaka et al. 1995; Loeb and Davies 1996a,b).

Several new descriptive terms (e.g., *side leakage, side illumination, channeling, plane-parallel albedo bias*) have been introduced by such studies in an attempt to explain the different effects of theoretical or observed cloud heterogeneity on radiative transfer. However, such terms have provided only a partial explanation of the mechanisms by which cloud heterogeneities affect radiation. As a result it has been difficult to explain the overall effects of cloud heterogeneity. Specifically, the main problems are as follows.

- Most terms have been used only in a qualitative sense,

* Current affiliation: University of Maryland, Baltimore County, Baltimore, Maryland.

Corresponding author address: Tamás Várnai, Climate and Radiation Branch, Code 913, NASA Goddard Space Flight Center, Greenbelt, MD 20771.
E-mail: varnai@climate.gsfc.nasa.gov

without exact definitions. Thus the magnitudes of various effects could not be quantified.
- Some definitions are applicable only to particular cloud geometries. For example, the term ''side illumination'' makes sense for hypothetical cuboidal or cylindrically shaped clouds but is harder to define when the distinction between cloud top and cloud side becomes blurred, as for many cumulus clouds.
- Each term tends to describe a single aspect of the effect of cloud heterogeneity on radiative transfer, independently of other aspects. It has been difficult, if not impossible, to relate such terms to each other or to assess their relative contribution to the overall effect of cloud heterogeneity.

Before proceeding to report new results on cloud heterogeneity, it appears worthwhile to first develop a more general theoretical framework for describing the effects of cloud heterogeneity on solar radiation. Section 2 therefore reexamines the main processes by which cloud heterogeneity affects radiative transfer. In particular, it identifies the main differences between photon trajectories that take place within heterogeneous, as opposed to homogeneous, clouds. This leads to the fundamental definitions of *escape* and *trapping,* which may be further divided into upward and downward components. These terms are then used in the rest of the paper to illustrate the overall effects of cloud heterogeneity on the reflection of single-layered cloud fields.

While most earlier studies used simple cloud geometries, such as cubes or cylinders, the focus has since shifted toward examining more realistic, stochastic cloud structures. In most cases, the stochastic cloud structure was specified by the horizontal distribution of optical thickness, τ, which was either retrieved from satellite images or generated by cloud models. Most studies of stochastic cloud fields have attributed all τ variations to changes in the volume extinction coefficient and have kept the cloud geometrical thickness constant (e.g., Barker and Davies 1992a; Marshak et al. 1995a,b; Gabriel and Evans 1996). Less attention has been given to the effect of stochastic variations in geometrical cloud thickness. Chambers et al. (1997) assumed that τ variations are due to changes not only in volume extinction coefficient but also in cloud-base altitude, and Hignett and Taylor (1996) included some of the effects of cloud-top height variability in their calculations. In addition, Duda et al. (1996) and Zuidema and Evans (1998) studied thin stratus and stratocumulus fields having slight cloud-top variability. Recently, Loeb et al. (1997, 1998) and Loeb and Coakley (1998) pointed out that some observations of stratus and stratocumulus cloud fields cannot be explained by assuming variations in only the volume extinction coefficient while keeping the cloud-top height constant. Everyday experience also indicates that the assumption of a constant cloud-top height is inappropriate for most cumulus cloud fields.

Therefore, the main purpose of this paper is to compare the effects of variations in volume extinction coefficient to those in cloud-top height. This study compares the overall effects and explains how these two types of cloud heterogeneity influence solar radiation. The theoretical framework developed in section 2 is used to quantitatively evaluate the individual mechanisms and to explain their differences for the two types of cloud heterogeneity.

The outline of this paper is as follows. First, section 2 introduces the theoretical framework used to examine radiative heterogeneity effects, then section 3 describes the way the magnitudes of various mechanisms are calculated for stochastic cloud fields. The individual mechanisms and their effects on scene albedo are examined in section 4, while the effects on reflection toward the zenith—a direction particularly important for satellite remote sensing—are investigated in section 5. In particular, section 5 seeks an explanation for the observations of Loeb and Davies (1996b), that cloud reflectivity toward the zenith increases with the solar zenith angle. Such behavior is contrary to that from a horizontally homogeneous cloud with no cloud-top height variability, leading Loeb et al. (1997) to suggest that it is caused by horizontal heterogeneity effects. Thus section 5 examines in detail how cloud heterogeneity causes such an increase. Finally, section 6 gives a brief summary and offers some concluding remarks.

2. Definitions of radiative heterogeneity effects

To explain the complex influence of cloud heterogeneities on shortwave radiation, the proposed framework uses three types of solution. The first one is a homogeneous, plane-parallel calculation using the scene-averaged cloud properties. The second is an approximation that integrates the one-dimensional radiative transfer solution over the area of a given scene, thereby accounting for the horizontal changes in cloud optical properties but not for the effects of horizontal transport of radiation between neighboring regions with different properties. As discussed below, this second approach is called the tilted independent pixel approximation (TIPA). The third approach is to obtain the full solution, which requires the application of a three-dimensional radiative transfer that includes the effects of horizontal transport without approximations.

Accordingly, the proposed framework distinguishes two different types of heterogeneity effects. The first, found using TIPA, is termed the *one-dimensional heterogeneity effect.* This is the difference between the one-dimensional integrated solution (e.g., an albedo or radiance value) and that for an equivalent homogeneous cloud field with the same average optical depth. The second is found by differencing the full three-dimensional solution and the approximate one-dimensional (TIPA) solution. Since this is a measure of the difference in results due to the effect of including horizontal transport between neighboring columns, it is termed the *hor-*

izontal transport effect. The sum of the one-dimensional heterogeneity effect and horizontal transport effect is termed the *three-dimensional heterogeneity effect* and is the difference between the full three-dimensional solution and its homogeneous, plane-parallel counterpart using horizontally averaged cloud optical properties.

a. The one-dimensional heterogeneity effect

For highly absorbing or very low-order scattering situations, the entire three-dimensional problem of cloud heterogeneity is solvable by integrating the direct beam reflection, absorption, and transmission over the relevant scene. This technique directly accounts for the nonlinear dependence of attenuation on cloud optical depth, as well as the effects of variable cloud geometry, and avoids the biases arising due to Jensen's inequality (Newman et al. 1995) when area-averaged cloud properties are used. The one-dimensional heterogeneity effect is then defined to be the difference between the answer obtained by integration over the area and that obtained from a single radiative transfer calculation, which uses the area-averaged cloud properties as input.

Although the general case involving higher orders of scatter is more complicated, it is still possible to use area integration to define the one-dimensional heterogeneity effect. In this case, each point is assigned the cloud properties that occur along the slant path of the direct beam that goes through the point. With this approach, the one-dimensional effect still describes the entire influence of cloud heterogeneity in the limit of (a) small optical depth, (b) strong absorption, or (c) weak horizontal heterogeneity.

A similar treatment has previously been used (e.g., Cahalan et al. 1994, 1995; Oreopoulos and Davies 1998) in calculating the plane-parallel albedo bias (PPAB) based on the independent pixel approximation (IPA). This approximation considers the local cloud properties in the vertical direction and integrates the results of one-dimensional radiative transfer over the relevant areas. By definition, the IPA and the PPAB disregard the net effects of horizontal photon transport. However, while the PPAB produces exact results for the one-dimensional effect for overhead sun (the exact relationship is PPAB $= -1$dh, with 1dh being the one-dimensional heterogeneity effect), it overestimates it for many cases of oblique illumination (even in the limit of strong absorption).

For example, the PPAB would estimate a strong one-dimensional heterogeneity effect for the case shown in Fig. 1 since the IPA assumes that half of the direct solar irradiance is unaffected by cloud (beams A, E, and F), whereas the other half encounters fairly thick clouds (beams B, C, and D). A more exact analysis of this example, however, shows that all photons will pass through some cloud. So for this case, the PPAB overestimates the one-dimensional heterogeneity effect since it overestimates the influence that the photons' initial positions have on whether they get reflected or transmitted.

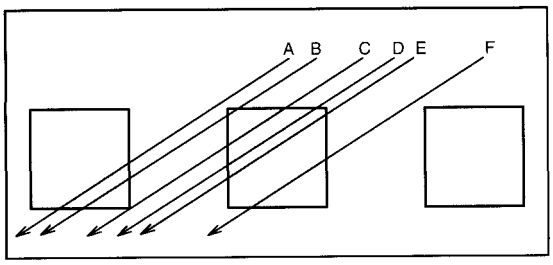

FIG. 1. Vertical cross section of a field of cuboidal clouds. The arrows indicate the paths of various direct beams.

Choosing the slant path through the cloud corresponding to each starting location mitigates most of the problems present in the IPA. This method assigns similar slant paths to both members of beam pairs AB and DE, and somewhat different thicknesses to the two members of beam pairs BC and EF. The relevant optical thickness τ^* for each starting location is found as

$$\tau^*(x_0, y_0) = \int_{z_{\text{bottom}}}^{z_{\text{top}}} \beta[x^*(z), y_0, z]\, dz, \qquad (1)$$

where z_{bottom} and z_{top} are the altitudes at the bottom and top of the cloud layer, $x^*(z) = x_0 - (z - z_{\text{top}}) \tan\Theta_0$, Θ_0 is the solar zenith angle, and (x_0, y_0) is the point where a photon enters the cloud layer (for convenience, in a direction perpendicular to the y axis). Then the influence of the one-dimensional heterogeneity effect on an entire scene's albedo can be calculated from the equation

$$1\text{dh} = \langle A[\tau^*(x, y)]\rangle - A(\langle\tau\rangle), \qquad (2)$$

where 1dh is the one-dimensional heterogeneity effect, $A(\tau)$ is the albedo of a plane-parallel cloud with τ optical thickness, and $\langle\ \rangle$ indicates averaging over the entire scene. The first term in the right-hand side of this equation can be calculated in two steps. First, the spatial distribution of τ^* values can be calculated by keeping track of the optical thickness that photons pass through in Monte Carlo simulations, if all the scattering angles are set to zero. Second, the appropriate albedos can be obtained much as in the IPA with τ^* substituted for τ. Since the τ^* values are optical thicknesses of thin columns tilted toward the sun, and the interactions of the tilted columns are not considered, the calculation of the first term on the right side of Eq. (2) can be called TIPA.

Although not specified in Eqs. (1) and (2), the effects of variations in microphysical cloud properties (i.e., phase function, single-scattering albedo, and gaseous volume absorption coefficient) can also be included by replacing $A(\tau^*)$ (the albedo of a single homogeneous cloud layer) by A^* (the albedo of a plane-parallel cloud with vertical heterogeneities) (Fig. 2).

Although the main purpose of the TIPA is to calculate

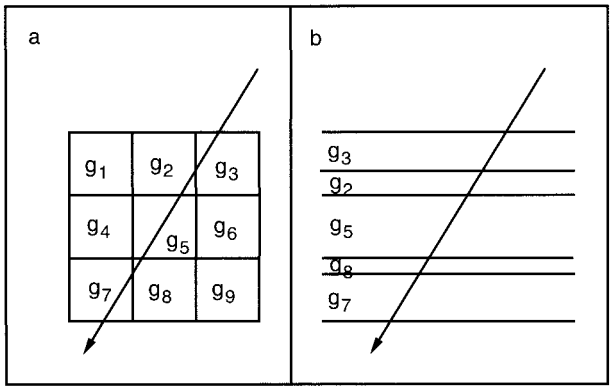

FIG. 2. Microphysical variations in the TIPA: (a) the real cloud with variable phase function asymmetry factor (g_1, g_2, . . . , g_9) and (b) the plane-parallel cloud that the beam is assumed to encounter in TIPA.

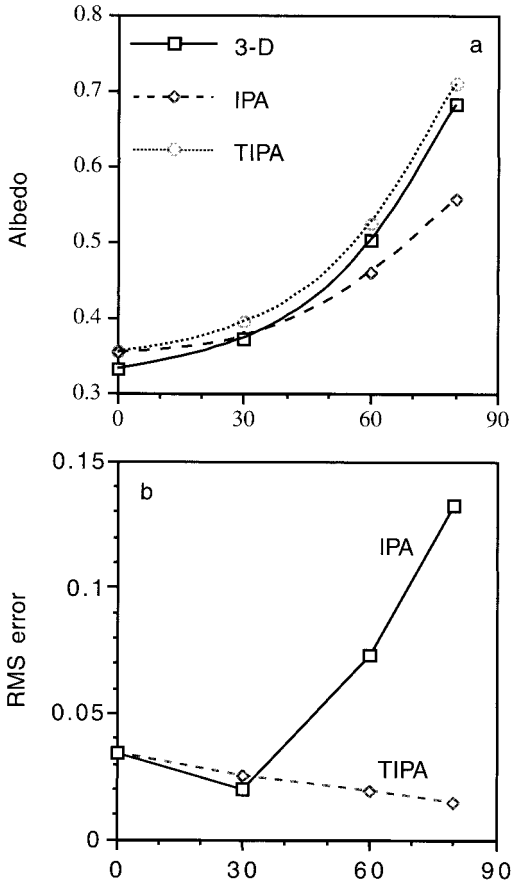

FIG. 3. (a) Average albedos for 54 irregular cloud fields generated by the stochastic model of Barker and Davies (1992a). At 69-m resolution, the scenes cover $(35.2)^2$ km areas. The scene average optical thickness varies from 5 to 30, the cloud fraction varies from 0.5 to 1, and the scenes include a wide range of scaling properties. (b) The rms errors of IPA and TIPA solutions for the 54 scenes are shown.

the one-dimensional heterogeneity effect (as opposed to obtaining quick albedo estimates), it is also interesting to compare the TIPA and IPA albedo estimates. By definition, the two approximations give identical scene-average albedo values for overhead sun. For oblique illumination, the calculation of τ^* values usually smooths the original τ values in the x direction. This smoothing results in τ^* having less variability than the original τ values and thus causes TIPA albedos to lie between the albedos calculated using the IPA and the albedos of homogeneous plane-parallel layers having the same scene-average optical depths. Since the IPA always gives lower albedos than the homogeneous plane-parallel approximation, it follows that TIPA albedos are higher than IPA albedos. For small solar zenith angles, since even the IPA tends to overestimate the real albedo, the higher TIPA estimates are even further from the correct albedos. For large solar zenith angles ($\Theta_0 \geq 50°$–$60°$), however, the IPA grossly underestimates the true albedo, and thus the TIPA estimates tend to be more accurate (Fig. 3). It should be noted that, although TIPA's average error over all scenes does not change significantly with the solar zenith angle, the error for most individual scenes either increases or decreases.

The difference between the IPA and the TIPA has been discussed above in terms of the cloud properties they assign to each solar beam. Their fundamental difference can also be described in terms of the distribution of incoming solar radiation: the IPA assigns equal amounts to all horizontal unit areas, whereas the TIPA assigns equal amounts to all unit areas that are perpendicular to the incoming solar radiation (Fig. 4). This fundamental difference results in the TIPA being able to explain qualitatively why cloud reflection properties depend not only on the frequency distribution of cloud optical thicknesses (as assumed by the IPA) but also on the spatial distribution of τ values. For example, the TIPA can help explain why wind shears toward and away from the sun result in different radiative effects (Barker 1994), or why cloud streets parallel and perpendicular to the solar illumination have different albedos (Davies 1976, p. 137).

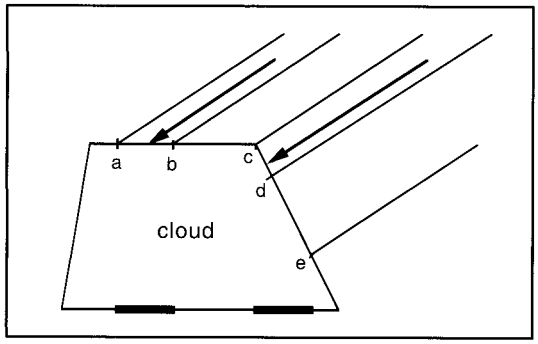

FIG. 4. A case showing that IPA assigns equal amounts of solar radiation to horizontal areas [intervals (a, b) and (c, e)], whereas TIPA assigns equal amounts to areas perpendicular to the incoming solar radiation [intervals (a, b) and (c, d)].

This feature makes the TIPA somewhat related to two one-dimensional radiative transfer approaches described in previous studies: an approach that uses an apparent cloud fraction, and one that treats direct and diffuse radiation separately.

As Snow (1985) and Minnis (1989) show, clouds in broken cloud fields appear to occupy increasing portions of a scene as it is viewed from increasingly oblique angles. The cloud fraction apparent from the sun's direction (CF_{app}) has been used in numerous radiative studies (e.g., Aida 1977; Kobayashi 1988; Barker 1994). The TIPA is closely related to this CF_{app} since both calculate the fraction of the incoming solar radiation that is intercepted by clouds, but TIPA extends the concept of the CF_{app}, which distinguishes only between cloud and no cloud, by also accounting for variations in cloud optical thickness.

The TIPA—in which all radiation moves obliquely—can also be regarded as an extension of Gabriel and Evans' (1996) IPA modified source (IPAMS), in which direct and diffuse radiation are separated assuming that the direct beam is tilted according to the solar elevation, whereas the diffuse radiation propagates in the vertical direction. Since this artificial separation at the first scattering event can cause problems in situations involving low-order scattering, TIPA is considered more appropriate than IPAMS for the purpose of calculating the one-dimensional heterogeneity effect. (For example, IPAMS gives the same results as the IPA if there is a thin cirrus layer above the heterogeneous clouds.)

The main limitation of the TIPA is of course that it is still a one-dimensional approach that ignores the effects of horizontal transport, and it cannot be used to examine phenomena that are inherently three-dimensional. For example, the TIPA cannot give accurate estimates for the angular distribution of radiation reflected from broken cloud fields since the enhanced backscatter from cloud sides (Davies 1976, p. 127; Wendling 1977) is not present in one-dimensional theory. Such problems can be solved only by considering the effects of horizontal radiative transport.

b. Mechanisms of the horizontal transport effect

The horizontal transport effect describes the differences from TIPA that arise when the total impact of cloud heterogeneity is included. (For overhead sun, this is analogous to considering the effects of horizontal transport on the IPA.) The main differences act to extend or shorten the photon pathlengths within the cloud field, effects that can be referred to as trapping or escape, respectively. (Because the relevant pathlengths are the optical pathlengths, their calculation requires an integration of the extinction coefficient over the physical pathlength.)

Earlier studies considered the influence of cloud heterogeneity on photon pathlengths mainly in the context of cloud absorption (e.g., Davies et al. 1984). However, the change in pathlengths can also be considered the fundamental effect through which heterogeneities influence cloud reflection and transmission for three reasons. First, the change in pathlengths can affect the amount of absorption, which determines how much radiation is available for reflection and transmission. Second, the change in pathlengths implies fewer or additional scattering events. This is important since scattering changes the direction in which photons move, and thus, the amount and angular distribution of both reflection and transmission. Third, the change in pathlengths influences where photons emerge from the cloud field, that is, the spatial distribution of cloud reflection and transmission.

The various cases of trapping can be separated into two categories, *upward* and *downward trapping,* according to whether the trapping hinders the emergence of a photon that would be reflected or transmitted in TIPA. Similarly, the escape effect can also be divided into upward and downward components, depending on whether the escape helps a photon emerge from the cloud layer in an upward or downward direction. As a result, four horizontal transport effects can be defined.

1) UPWARD TRAPPING, UT

Here the TIPA solution allows the photon to be reflected after a total optical pathlength of l_{1d}, whereas in the real cloud, additional scattering occurs with a total pathlength of $l_{3d} > l_{1d}$. Since upward trapping makes it more difficult for radiation to be reflected, it tends to decrease the cloud albedo. Two examples of upward trapping are given in Fig. 5a. In these examples the photon does not escape upward after traversing the pathlength traveled in TIPA because it either encounters more cloud with the same extinction coefficient (e.g., higher cloud tops) or a region with a larger extinction coefficient. Special cases of the upward trapping effect have previously been described as ''side illumination'' (Wendling 1977; Kobayashi 1993).

2) DOWNWARD TRAPPING, DT

This is analogous to upward trapping, but it increases the pathlengths of those photons that are transmitted in the TIPA. The extra pathlength now acts to decrease the transmission. Two examples of downward trapping are shown in Fig. 5b, one for increased geometrical thickness, the other for increased extinction coefficient. Note from the first of these examples that horizontal transport can at times be sufficiently complicated that it may produce slightly counterintuitive results. Here the photon moves horizontally to a region with less thickness, yet the result is trapping since the scattering takes the photon back to a higher altitude region of the thicker column.

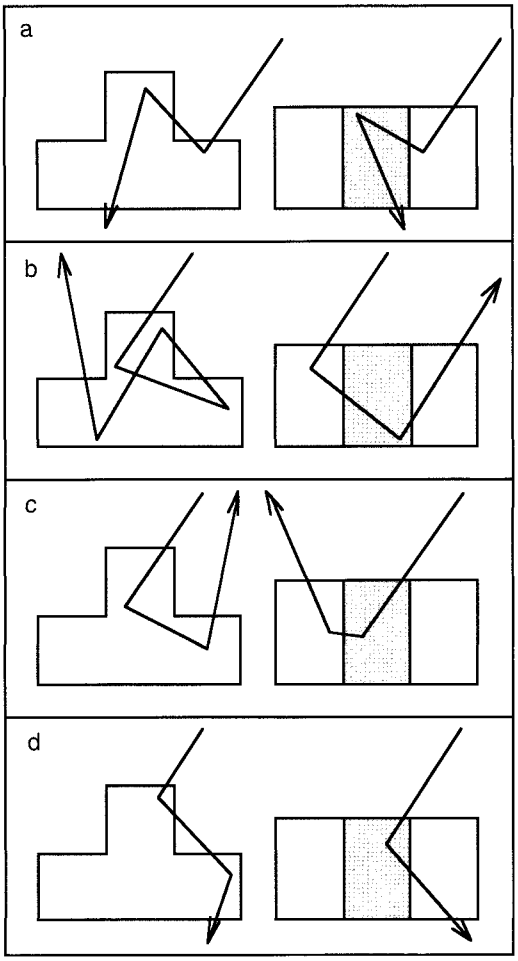

FIG. 5. Paths of photons that experience horizontal transport effects in clouds having cloud-top height and volume extinction coefficient variations: (a) upward trapping, (b) downward trapping, (c) upward escape, and (d) downward escape. Denser shading indicates a higher volume extinction coefficient.

3) UPWARD ESCAPE, UE

This is the opposite of upward trapping and occurs when the photon emerges with a total pathlength $l_{3d} < l_{1d}$. In this case, the shorter pathlength acts to increase cloud reflection. Two examples of upward escape are shown in Fig. 5c. This effect has previously been described for simple cloud geometries by Davies (1978) and Kobayashi (1993) to explain increases in cloud reflectivity into oblique upward directions.

4) DOWNWARD ESCAPE, DE

The final possibility is for the photon to escape downward with a shorter pathlength than in the TIPA, acting to increase transmission. Examples of downward escape are show in Fig. 5d. This effect has previously been described for plane parallel clouds with a horizontally variable extinction coefficient by Cannon (1970), who termed the effect *channeling.*

c. Net influence of horizontal transport

The mechanisms described above apply to general cloud radiative transfer problems that may include the effects of absorption, or examine the horizontal distribution of the emerging radiance, etc. For some studies, however, details of the photon pathlength distribution may be irrelevant, and all that may be needed is the net result for the horizontally averaged reflected or transmitted fluxes and radiances. For example, if a photon affected by upward trapping still emerges in the upward direction, only with a longer pathlength than in the TIPA, this may be of no special interest to such studies.

Accordingly, one may define the net effects of upward and downward trapping, called net upward trapping (NUT) and net downward trapping (NDT), respectively. Net upward trapping is defined as the change in the albedo (or radiance, etc.) value because a portion of the solar radiation affected by upward trapping fails to contribute to the albedo (or radiance, etc.), and net downward trapping, as the change in the radiative value of interest because a portion of the solar radiation affected by downward trapping fails to contribute to transmission. One can similarly define net upward escape (NUE) and net downward escape (NDE) as the changes in the albedo (or radiance, etc.) due to upward and downward escape, respectively.

These definitions complete the theoretical framework proposed in this paper, as summarized in Tables 1, 2, and 3.

3. Calculation of heterogeneity effects

a. General approach

Having defined the different terms that are needed to describe the radiative effects of cloud heterogeneity, this section addresses how these may be calculated using a radiative transfer model. The conventional Monte Carlo approach determines the random paths of simulated pho-

TABLE 1. Relationships among various heterogeneity effects.

3D heterogeneity effect	= 3D solution − homogenous solution
1D heterogeneity effect	= TIPA solution − homogenous solution
Horizontal transport effect	= 3D solution − TIPA solution
3D heterogeneity effect	= 1D heterogeneity effect + horizontal transport effect
Horizontal transport effect	= net upward trapping + net downward trapping + net upward escape + net downward escape

TABLE 2. The influence of each component of the horizontal transport effect on individual photons.

Component	Real photon		Photon assumed in TIPA
Upward trapping (UT)	l_{3d} can be either reflected, transmitted, or absorbed	$>$	l_{1d} is reflected
Downward trapping (DT)	l_{3d} can be either reflected, transmitted, or absorbed	$>$	l_{1d} is transmitted
Upward escape (UE)	l_{3d} is reflected	$<$	l_{1d} can be either reflected, transmitted, or absorbed
Downward escape (DE)	l_{3d} is transmitted	$<$	l_{1d} can be either reflected, transmitted, or absorbed

TABLE 3. Summary of photons contributing to each component of the net horizontal transport effect on albedo.

Component	Real photon		Photon assumed in TIPA
Net effect of upward trapping on albedo (NUT)	l_{3d} can be either transmitted, or absorbed	$>$	l_{1d} is reflected
Net effect of downward trapping on albedo (NDT)	l_{3d} is reflected	$>$	l_{1d} is transmitted
Net effect of upward escape on albedo (NUE)	l_{3d} is reflected	$<$	l_{1d} can be either transmitted, or absorbed
New effect of downward escape on albedo (NDT)	l_{3d} is transmitted	$<$	l_{1d} is reflected

tons in a given cloud (having a designated three-dimensional distribution of extinction coefficient, single-scatter albedo, and scattering phase function). Since this involves simulating the individual photon pathlengths that are needed to calculate the various components of the horizontal transport effect, the Monte Carlo approach is particularly suitable for simultaneously calculating both the one-dimensional heterogeneity effect and the horizontal transport effect.

The photon starting locations are chosen from a uniform horizontal distribution. Each starting location has an associated slant path through the cloud in the direction of the incident illumination, which determines the initial vertical distribution of extinction coefficient, single-scatter albedo, and phase function. At this stage the results from the TIPA could simply be calculated using any good one-dimensional model, and the results integrated over the horizontal variability of the starting locations. However, in order to calculate both the one-dimensional heterogeneity effect and the horizontal transport effect, it is advantageous to continue with a Monte Carlo simulation even for the one-dimensional heterogeneity effect. The TIPA simulation proceeds by assuming that the slant path properties (chosen separately for each photon) are fixed horizontally and that the cloud layer boundaries (as defined by the slant path) are plane parallel.

At the same time, a second simulation takes place that follows the path of the same photons but which includes the complete three-dimensional heterogeneity. By choosing identical random number sequences for each photon pair in the TIPA and the fully three-dimensional simulations, the differences in the photon pathlengths can be attributed to the effects of cloud heterogeneity.

At the end of the simulations, the one-dimensional heterogeneity effect can be calculated from the results of the TIPA simulation alone, based on Eq. (2). The various components of the horizontal transport effect, in turn, can be obtained from comparing the l_{1d} and l_{3d} pathlengths each photon traveled in the two simulations. For example, the amount of radiation affected by upward trapping can be calculated from the percentage of photons reflected in the TIPA simulation for which $l_{3d} > l_{1d}$, and net upward trapping, from the percentage of these affected photons, which do not get reflected in the three-dimensional simulation.

The above method examines how photons are influenced by heterogeneities as they move along their paths within the cloud layer. This approach is different from the one used in previous studies, which focused on how heterogeneities influence the radiation field at various fixed locations. For example, Davis (1992), Marshak et al. (1995a), Gabriel and Evans (1996), Davis et al. (1997), and Chambers et al. (1997) examined the radiation at points of various densities within a cloud with volume extinction coefficient variations; and McKee and Cox (1974), Davies (1976, 1978), Aida (1977), Welch and Wielicki (1984), and Bréon (1992) studied the radiation that left cuboidal and cylindrical clouds through their tops and, separately, their sides. The difference between the present approach and other ones is analogous to the difference between the Lagrangian and Eulerian approaches used, for example, in fluid dynamics.

b. Specific experiments

This study analyzes radiative effects of heterogeneous cloud fields. Some fields were retrieved from satellite images, and some were generated by a stochastic cloud model. It uses six optical thickness fields retrieved by Oreopoulos (1996) from visible Landsat–TM images.

TABLE 4. Input parameters for a set of artificially generated cloud fields. A separate cloud field has been generated for each possible configuration of input parameters.

Parameter	Input value(s)
Horizontal resolution	68.75 m
Domain size	$(35.2 \text{ km})^2$
Scene-average optical thickness	5, 15, 30
Cloud fraction	0.5, 0.75, 0.98
Set of scaling parameters*	(1.5, 4.0, 6), (1.0, 3.6, 10), (1.0, 3.0, 12)

* The three parameters are scaling before and after scale break, and wavenumber at scale break. For exact definitions, see Barker and Davies (1992a).

The scenes cover $(57.3 \text{ km})^2$ areas at a resolution of 28 m and contain cumulus and stratocumulus clouds over ocean. (For computational reasons, each scene is divided into four rectangular segments, leading to 24 small subscenes.) The average cloud optical thickness (retrieved from the measured radiance using a one-dimensional model) varies between 2.8 and 18. The cloud fraction CF varies between 0.13 and 1.

To increase the variety of the available scenes, some artificial cloud fields generated by the model of Barker and Davies (1992a) are also examined. To keep the generated cloud fields similar to observed satellite images, an optional scaling break has been added to Barker and Davies' original model. It should be noted, however, that while scaling breaks appeared on visible and infrared satellite images (e.g., Cahalan and Snider 1989; Barker and Davies 1992b; Davis et al. 1997), as well as in lidar measurements of cloud top–height variations (Boers et al. 1988), they were not detected in liquid water path measurements (Cahalan and Snider 1989) nor in radar reflectivities (Tessier et al. 1993). Therefore, the origin of the observed breaks remains the subject of continued research (Cahalan 1989; Marshak et al. 1995a, 1998; Davis et al. 1997).

A total of 27 artificial τ fields were generated using the input parameters listed in Table 4. As the table shows, these scenes include a wide variety of cloud structures from thin to thick and from nearly homogeneous to highly heterogeneous broken cloud scenes. An example of the generated cloud fields is shown in Fig. 6. While this set of artificial scenes does not represent the full variety of real clouds, it does allow the study of features that may not be very pronounced in the available Landsat scenes. However, since it is not clear how representative the artificial fields are of real clouds, only the main features of the results are analyzed, and only qualitative conclusions are drawn from the numerical results. Additionally, the use of Landsat scenes is expected to prevent the drawing of any conclusions that would be specific to the adopted stochastic cloud model.

Radiative transfer through the cloud fields is modeled using the Monte Carlo model described in Várnai (1996). Simulations are presented tor 0.865-μm wavelength, assuming conservative scattering. The phase function of cloud droplets is calculated for 0.865 μm based on Mie theory, using the Sc_{top} cloud drop size distribution of Welch et al. (1980). The effects of the surrounding atmosphere and underlying surface are not considered. The experiments presented in sections 3 and 4 simulated 10^5 and 5×10^5 photons, respectively. Following Davies (1978), the σ statistical uncertainty of a result value V (e.g., albedo, or the ratio of photons affected by downward escape) can be calculated using the equation

$$\sigma_V = [V(1 - V)N_{\text{total}}^{-1}]^{1/2},$$

where N_{total} is the number of simulated photons. For the reflectance values presented in section 5, V in the above equation should be multiplied by $(0.251\mu)/\pi$, where μ is the cosine of the viewing zenith angle. (The Monte Carlo program yields reflectance values based on the flux reflected into a solid angle equal to 0.251 sr.)

4. Effects on scene albedo

When only the horizontal distribution of cloud optical depth is available (e.g., from visible satellite images), one can attribute the variations to changes in either the cloud geometrical thickness or the cloud volume extinction coefficient. This section examines the mechanisms through which these two types of heterogeneity influence solar radiation and compares their effect on the scene albedo.

The most appropriate way to compare the effects of the two kinds of cloud heterogeneity is to consider the same horizontal τ distributions, average geometrical thicknesses, and average volume extinction coefficients for both approaches. Accordingly, two cloud fields were generated for each of the τ fields described in section 3. For clouds with variable geometrical thickness, the cloud-top height was determined from

$$z(x, y) = \frac{\tau(x, y)}{\beta}, \tag{3}$$

where $\beta = 30 \text{ km}^{-1}$ is the cloud volume extinction coefficient (constant throughout the scene). (The cloud base is assumed to be at $z = 0$ for all scenes.) The corresponding scenes with volume extinction coefficient variations were generated using

$$\beta(x, y) = \frac{\tau(x, y)}{\langle z \rangle},$$

where $\langle z \rangle$ is the average value of the cloud-top heights determined from Eq. (3) (not including the cloud-free pixels). The geometrical thickness of fields with extinction variations is set to $\langle z \rangle$.

a. Overhead sun

For overhead sun, the one-dimensional heterogeneity effect depends only on the optical thickness distribution

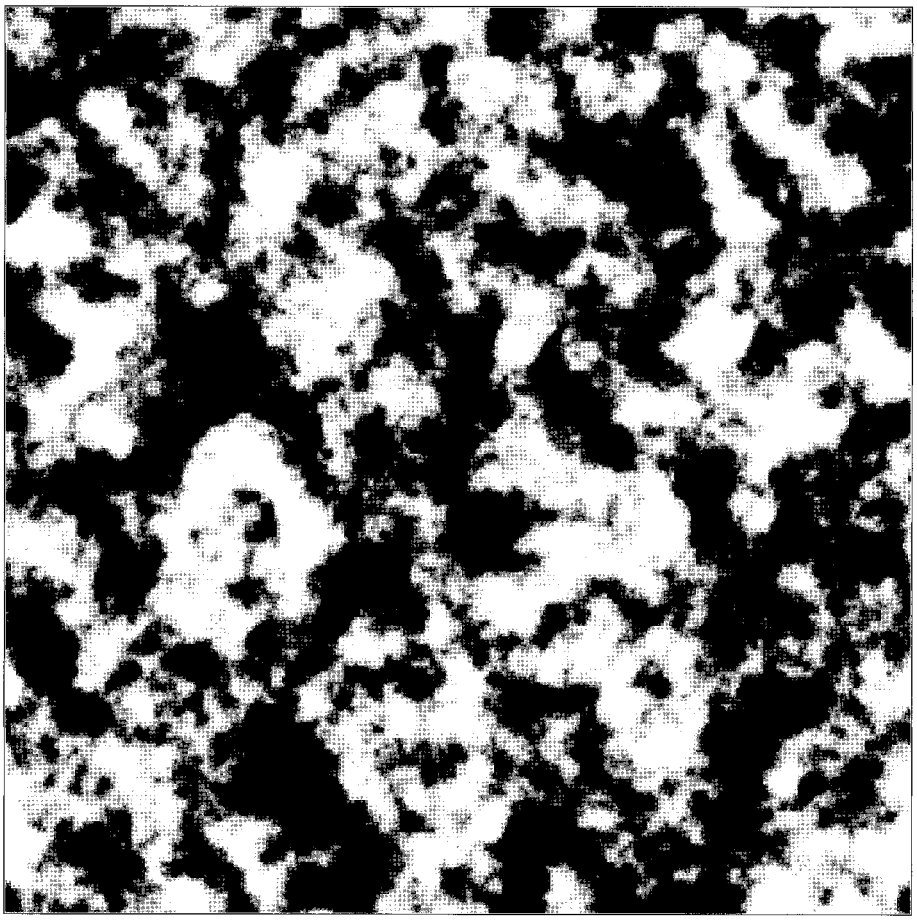

FIG. 6. A cloud field generated using the stochastic cloud model. The cloud field, covering an area of (35.2 km)^2 at a resolution of 68 m, was generated using the input parameters CF = 0.75, $\langle\tau\rangle = 15$, $s_k = 1$ if $k \leq 10$, and $s_k = 3.6$ if $k > 10$. (Here s is the scaling parameter and k is the wavenumber.) The optical thickness varies between 0 and 85 with a standard deviation of 28. For 0° and 60° solar zenith angles, the average scene albedos are 0.35 and 0.51, respectively. (The albedos of a homogeneous cloud with $\langle\tau\rangle = 15$ would be 0.50 and 0.66 for the two solar zenith angles.) The brightness of each pixel is proportional to its albedo, as calculated for overhead sun using IPA.

and is thus identical for both types of cloud heterogeneity. However, Fig. 7 shows that cloud-top height variability causes a much stronger horizontal transport effect than volume extinction coefficient variability does. Another difference between the two types of heterogeneities is that although the albedo is reduced in most cases, it is increased for slight cloud-top (but not extinction) variations. This increase, always less than 0.01, can be attributed to the relatively strong upward escape effect of cloud-top height variations.

The reasons for these differences are explained below, using the τ-field shown in Fig. 6 as an example. The magnitudes and efficiencies of various heterogeneity effects occurring in this field are summarized in Table 5, the efficiencies being defined by

$$\text{Efficiency} = \frac{|\text{net effect}|}{\text{ratio of affected radiation}}.$$

1) UPWARD TRAPPING, UT

The effects of upward trapping can be studied by considering a photon that enters a thin pixel of optical thickness τ_1, descends in that pixel through an optical distance τ_d, and then moves to an optically thicker neighboring pixel with $\tau_2 > \tau_1$ (Figs. 8a,b). The fact that upward trapping affects only about 11% more radiation for cloud top than for extinction variations, whereas the difference in net effects is about 270%, indicates that the main difference is not in the amount of radiation that goes from pixel 1 to pixel 2, but in the different efficiency of upward trapping once the radiation moves to pixel 2. This efficiency depends on τ_{up}, the net optical thickness through which radiation must ascend to emerge from the cloud layer. More radiation gets turned downward again and transmitted to the underlying surface for larger values of τ_{up}, which results

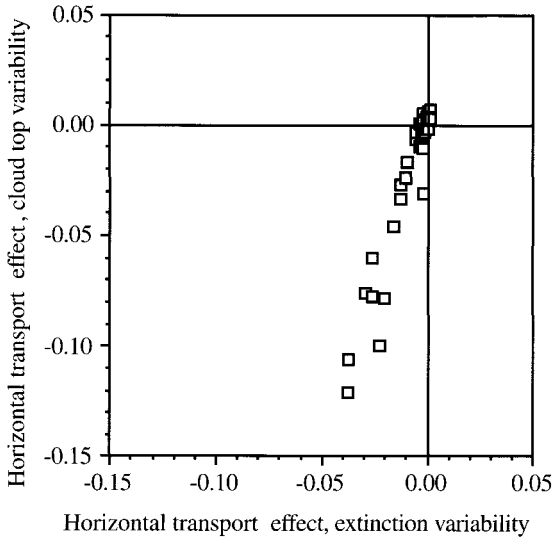

FIG. 7. Overall horizontal transport effects on the scene albedo due to cloud-top and extinction variations for overhead sun.

in a stronger net upward trapping. For cloud-top height (CTH) variations, τ_{up} is given by

$$\tau_{\text{up}}^{\text{CTH}} = \tau_2 - (\tau_1 - \tau_d),$$

whereas for volume extinction coefficient (VEC) variations, it is given by

$$\tau_{\text{up}}^{\text{VEC}} = \tau_2 - (\tau_1 - \tau_d)\frac{\beta_2}{\beta_1}.$$

Since $\beta_2 > \beta_1$, $\tau_{\text{up}}^{\text{CTH}} > \tau_{\text{up}}^{\text{VEC}}$, which implies a stronger upward trapping effect for cloud top than for extinction variations.

2) DOWNWARD TRAPPING, DT

Table 5 shows that downward trapping is a very weak effect for cloud-top variations. The reason for this is that radiation has to turn around twice (to move upward and then to move downward again) and go over the cloud top between its two ''U-turns'' (Fig. 5b), which does not happen very often. In the case of extinction variations, however, even a single change in a photon's direction may result in downward trapping (Fig. 5b).

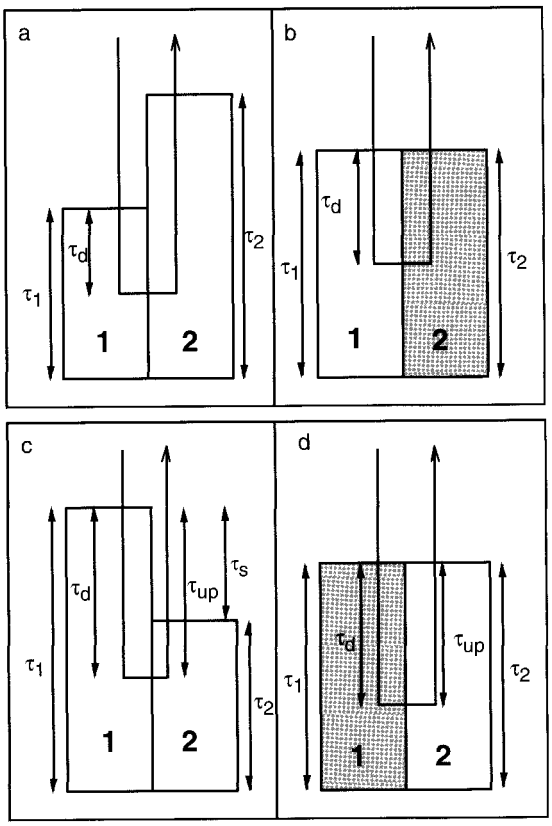

FIG. 8. Two-column models for horizontal transport effects due to cloud-top and extinction variations. Denser shading indicates higher volume extinction coefficient. (a)–(b) Upward trapping and (c)–(d) upward escape.

That is why downward trapping is much stronger for extinction than for cloud-top variations.

3) UPWARD ESCAPE, UE

As Table 5 shows, the amount of radiation affected by upward escape is similar for both cloud-top and extinction variations. Therefore, the explanation for the twofold difference in their net effects is found by considering whether the affected photons would also be reflected without the heterogeneities. This depends mainly on the $\tau_s = \tau_d - \tau_{\text{up}}$ optical thickness that, due

TABLE 5. Components of the horizontal transport effect for the cloud field shown in Fig. 6. The one-dimensional heterogeneity effect on scene albedo is −0.127.

	Cloud-top variations			Extinction variations		
Horizontal transport effect component	Ratio of affected photons	Net effect on scene albedo	Efficiency	Ratio of affected photons	Net effect on scene albedo	Efficiency
Upward trapping	0.162	−0.026	0.160	0.146	−0.010	0.068
Downward trapping	0.019	0.002	0.105	0.150	0.017	0.123
Upward escape	0.192	0.031	0.161	0.179	0.016	0.089
Downward escape	0.134	−0.030	0.224	0.205	−0.034	0.166
Total	0.544	−0.023	0.042	0.680	−0.011	0.016

to heterogeneities, is ''skipped'' by the affected photons. A larger τ_s value means that more of the affected photons would be turned downward again if there were no heterogeneities. For cloud-top variations (Fig. 8c),

$$\tau_{\text{up}}^{\text{CTH}} = 0, \quad \text{if } \tau_d \leq (\tau_1 - \tau_2) \quad \text{and}$$

$$\tau_{\text{up}}^{\text{CTH}} = \tau_2 - (\tau_1 - \tau_d), \quad \text{if } \tau_d > (\tau_1 - \tau_2).$$

For extinction variations (Fig. 8d),

$$\tau_{\text{up}}^{\text{VEC}} = \tau_2 - (\tau_1 - \tau_d)\frac{\beta_2}{\beta_1} = \tau_2 - (\tau_1 - \tau_d)\frac{\tau_2}{\tau_1}.$$

Since $\tau_2 < \tau_1$, $\tau_{\text{up}}^{\text{VEC}} > \tau_{\text{up}}^{\text{CTH}}$ for any τ_d value. In turn, $\tau_s^{\text{CTH}} > \tau_s^{\text{VEC}}$, which means that ascending photons ''skip'' more cloud particles in the case of cloud-top variations. Thus for extinction variations, most of the photons affected by upward escape would get reflected anyway, whereas for cloud-top variations, upward escape enables the reflection of many photons that would have been turned downward to the surface, if they had not skipped τ_s^{CTH}. This explains why upward escape is more efficient for cloud-top than for extinction variations.

Note that although, for the sake of clarity, Figs. 8c and 8d display a scattering event in pixel 2, this event is not necessary if the scattering in pixel 1 turns the photon by more than 90°, so that it is already moving upward by the time it enters pixel 2. This fact, and the equations above, both show that the two-column model allows for τ_2 to be zero, that is, that the model can be applied not only in the middle of clouds but also at cloud edges.

4) DOWNWARD ESCAPE, DE

Table 5 shows that downward escape affects more radiation for extinction variations than for cloud-top variations. The reason is that for variability in the extinction coefficient, downward escape can influence photons that move horizontally at any altitude, whereas for cloud-top variability, it can affect only those photons that move horizontally above the cloud top (Fig. 5d).

However, the fact that photons affected by downward escape start moving horizontally at higher altitudes for cloud-top (than for extinction) variability, also implies that these photons travel longer horizontal distances before they reach the cloud base. Since they tend to move toward thinner regions (they are affected by escaping rather than trapping), the fact that they travel longer distances means that they arrive to thinner and thinner areas and hence experience a more effective downward escape. As a result, downward escape can be expected to be more efficient for cloud-top variations than for extinction variations, which is in accordance with the data in Table 5. (In the particular cloud field examined, photons affected by downward escape travel about 56% farther for cloud-top than for extinction variability, which allows them to skip 47% more cloud particles, and hence escape more efficiently.)

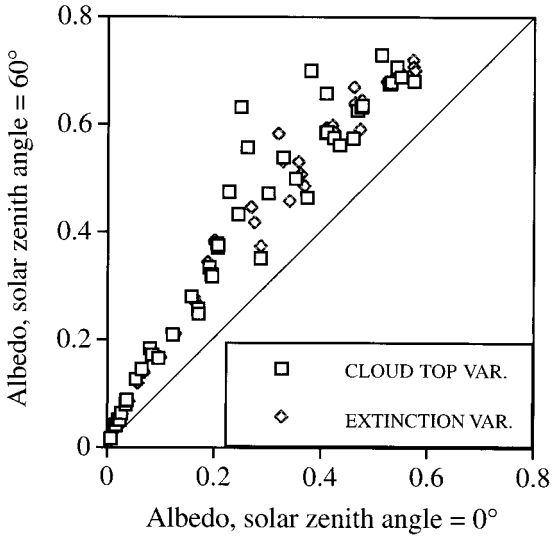

FIG. 9. Albedo of the examined scenes for overhead and oblique sun.

b. Oblique sun

Numerous studies indicate that the radiative effects of cloud heterogeneity change significantly with solar zenith angle (Θ_0). This section examines how cloud heterogeneity affects solar radiation for oblique sun.

Similarly to homogeneous scenes, the albedo of heterogeneous scenes increases with Θ_0 (Fig. 9). The figure also indicates that the rate of albedo increase varies widely among the individual scenes. The reason the observed increases do not follow a simple pattern is that they reflect changes in numerous processes; that is, the overall changes cannot be attributed to a single cause. This implies that in order to understand the overall changes, one has to consider how all the individual processes change with solar elevation.

The first reason for the albedo increase is that according to one-dimensional radiative transfer theory, cloud reflection increases with Θ_0 even if there are no heterogeneity effects. This increase is then further enhanced by the fact that since cloud fields tend to appear more homogeneous from oblique directions than from above, the one-dimensional heterogeneity effect (reducing cloud reflection) decreases with increasing Θ_0 for both cloud-top and extinction variations (Fig. 10).

However, as Fig. 11 shows, the horizontal transport effect (relative to TIPA) can either increase or decrease with the solar zenith angle, thereby further enhancing or reducing the overall albedo increase. Although there is no clear trend in the overall horizontal transport effect, there is one for each of its individual components. Changes to the overall horizontal transport effect thus depend on the balance of changes in the individual com-

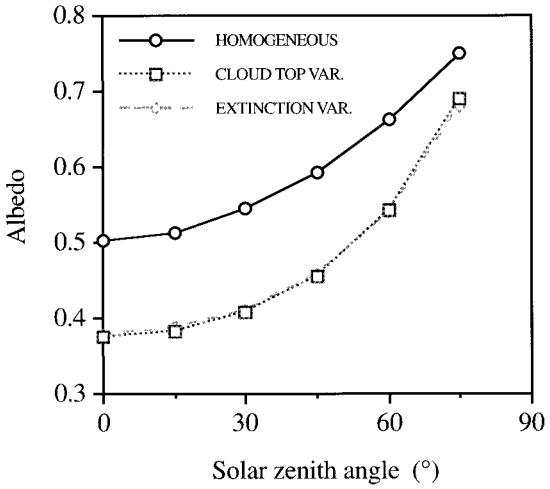

FIG. 10. Solar zenith angle dependence of albedos obtained for the cloud field shown in Fig. 6. The albedos are calculated using the homogeneous, plane-parallel approximation and TIPA.

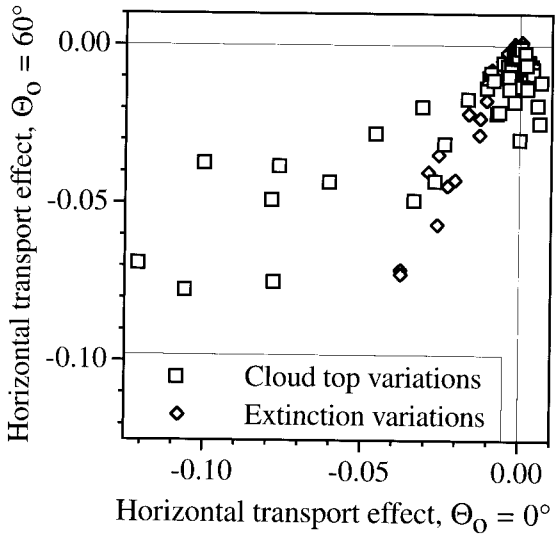

FIG. 11. Influence of horizontal transport effects on scene albedo.

ponents. (Figure 11 also shows that while the differences between the horizontal transport effects in fields with cloud-top and extinction variations remain significant, these differences tend to be smaller for oblique than for overhead sun.)

Figure 12 displays how the individual components of the horizontal transport affect change with solar zenith angle for the cloud field shown in Fig. 6. Examining the figure reveals that the changes are due mainly to variations in the amount of radiation (normalized by $\cos\Theta_0$) influenced by each component rather than to changes in the components' efficiency. As a general trend, this amount can be expected to increase with Θ_0 since clouds intercept more radiation for oblique sun and thus make more radiation potentially available for horizontal transport. However, other factors also influence the way each component of the horizontal transport effect depends on solar elevation. The main factors for the individual components are as follows.

1) UPWARD TRAPPING

The radiation that is potentially available for upward trapping is that which would be reflected in the TIPA. This amount increases with Θ_0 because more radiation is intercepted by clouds and also because the reflection of even a homogeneous, plane-parallel cloud increases with Θ_0.

In addition, as Θ_0 increases, cloud sides tilted toward the sun intercept more of the total incoming radiation, whereas cloud sides tilted away from the sun intercept less radiation; that is, $Y_{\mathrm{CTH}} > X_{\mathrm{CTH}}$ in Fig. 13. Since cloud particles scatter predominantly in forward directions, the majority of incident photons move to thicker cloud portions before being scattered upward and hence experience the upward trapping effect. Figure 13 also indicates that the part of cloud that gets thicker in the forward direction tends to intercept less radiation for extinction than for cloud-top variations; that is $(Y_{\mathrm{VEC}})/(X_{\mathrm{VEC}}) < (Y_{\mathrm{CTH}})/(X_{\mathrm{CTH}})$. Hence, this process can be expected to increase upward trapping less for extinction than for cloud-top variations, which is in accordance with the tendency in Fig. 12.

2) DOWNWARD TRAPPING

Figure 12 indicates that for cloud-top variations, downward trapping increases steeply with Θ_0. This happens because, for overhead sun, two U-turns are required for a photon to experience downward trapping (Fig. 5b), whereas for oblique sun, even a slight downward change in a photon's direction may result in downward trapping for direct beams that graze the upper edge of a cloud. For clouds with extinction variations, on the other hand, any small scattering angle can cause downward trapping, regardless of Θ_0. As a result, the amount of affected radiation does not change much with Θ_0.

A comparison of Figs. 12b and 12d reveals that for extinction variations, the efficiency of downward trapping increases with Θ_0. A possible explanation for this increase can be obtained by considering that as the sun becomes more oblique, enhanced multiple scattering moves the photons potentially available for downward trapping (i.e., the photons that would be transmitted without downward trapping) farther away from their paths assumed in TIPA (Fig. 14). These larger deviations imply that the photons experiencing downward trapping can get to regions where the extinction coefficient is much larger than it is along the path assumed in TIPA, and so they can experience more effective downward trapping.

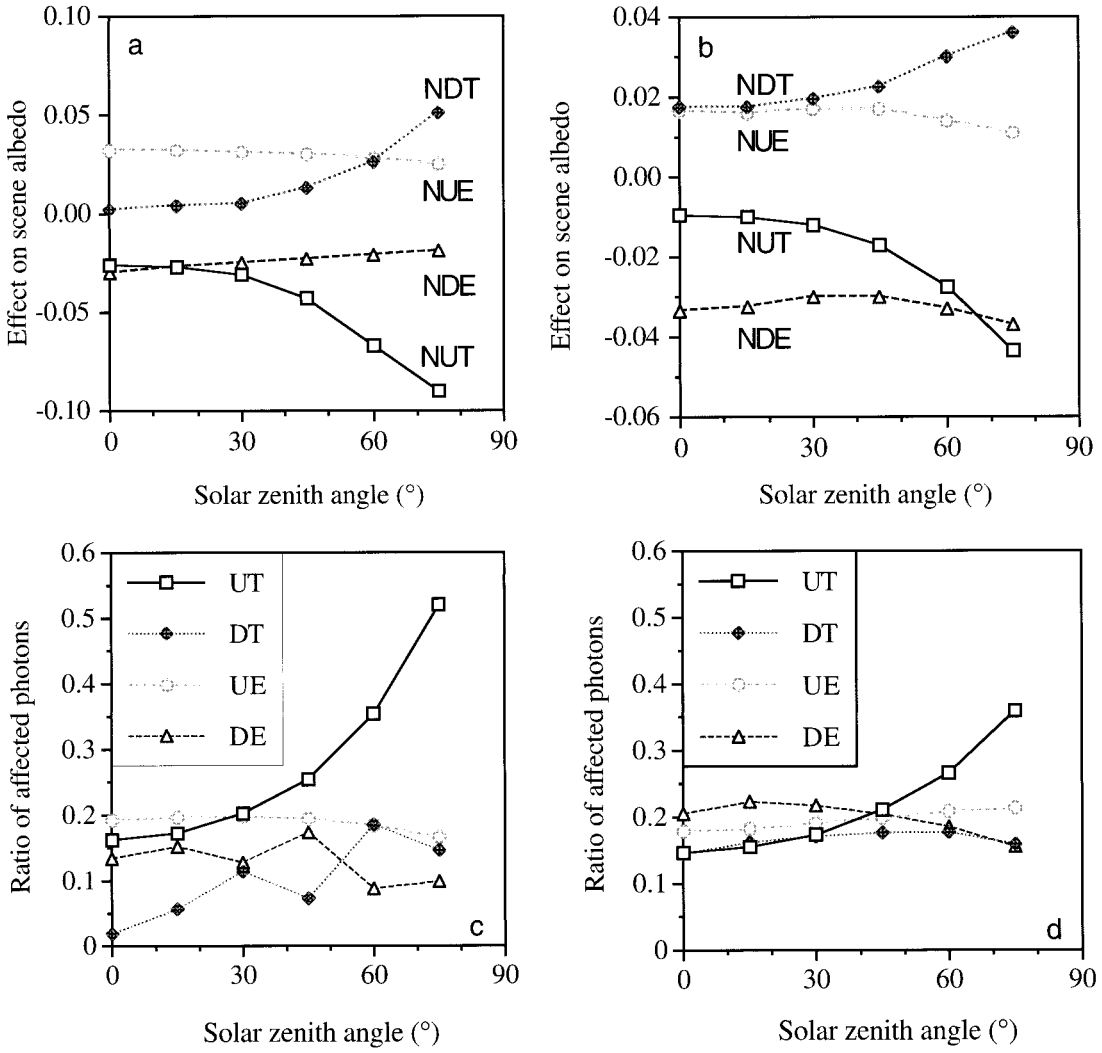

FIG. 12. Components of the horizontal transport effect for the cloud field shown in Fig. 6: (a) effect on scene albedo for cloud-top variations, (b) effect on scene albedo for extinction variations, (c) ratio of affected photons for cloud-top variations, and (d) ratio of affected photons for extinction variations (UT = upward trapping, DT = downward trapping, UE = upward escape, DE = downward escape, NUT = net upward trapping, NDT = net downward trapping, NUE = net upward escape, NDE = net downward escape).

3) UPWARD ESCAPE

The radiation potentially available for upward escape is simply that which is intercepted by clouds, regardless of whether it would be reflected or transmitted without horizontal transport. However, Fig. 12 shows that, although this potential radiation increases with Θ_0, upward escape nevertheless remains fairly constant. This can be explained by considering that the potentially available radiation (i.e., radiation intercepted by clouds) increases due to the extra radiation intercepted by cloud sides. Most of this radiation, however, moves forward, toward thicker regions, and hence tends to experience upward trapping rather than escape.

4) DOWNWARD ESCAPE

As with upward escape, the radiation potentially available for downward escape is that which is intercepted by clouds (regardless of whether it would be reflected without horizontal transport), which increases with Θ_0. Since photons tend to sink into clouds less at larger solar zenith angles, the downward radiation in clouds does not increase with the amount of intercepted radiation; this is probably why downward escape does not change much with Θ_0 (Figs. 12a,b).

c. Synthesis of individual components of the horizontal transport effect

Having examined the differences in the individual components of the horizontal transport effect, let us now synthesize these differences to observe some major tendencies for the two types of cloud heterogeneity. (As mentioned previously, all horizontal transport effects are relative to TIPA.)

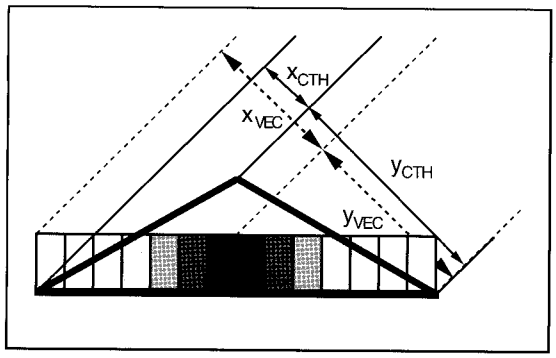

FIG. 13. Amount of solar radiation intercepted by the two sides of simple clouds. The optical thickness increases linearly toward the cloud center. The clouds with cloud-top (thick line) and extinction variations (shaded rectangle) have the same τ distribution and average geometrical thickness (CTH = cloud-top height variability and VEC = volume extinction coefficient variability).

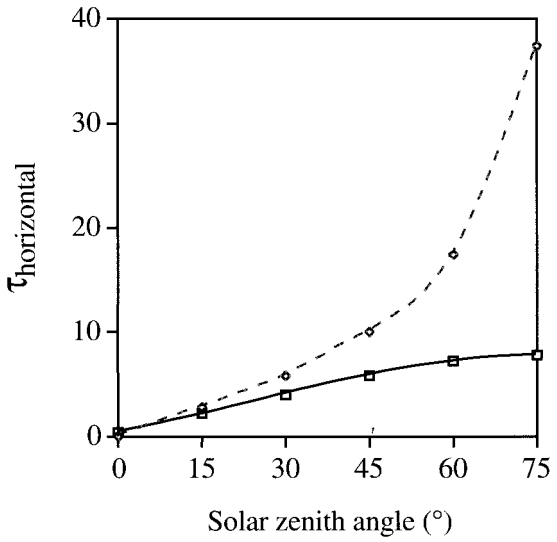

FIG. 14. Average distance (measured in optical thickness) between the x coordinates of points where transmitted photons enter the cloud top and leave the cloud base. (The x axis is parallel to the solar azimuth.) The dashed line is the distance assumed by TIPA, the solid line is obtained through three-dimensional Monte Carlo simulations for a homogeneous cloud with $\tau = 10$.

Radiation flowing from thinner to thicker cloud portions can be affected by upward or downward trapping, whereas photons moving from thicker to thinner areas can be affected by upward or downward escape. Thus, the net effects of radiation flowing toward thicker or thinner areas can be calculated by adding up the net influence of the two trapping and the two escape possibilities.

Since downward escape is by far the strongest component of the horizontal transport effect for extinction variations (Table 5), such variations lower the albedo mainly through radiation flowing from thick to thin areas [i.e., (NUE + NDE) − (NUT + NDT) < 0 in Fig. 15]. However, Fig. 15 also shows that the flow from thin to thick regions (NUT + NDT) is the dominant effect in lowering the albedo for most scenes with cloud-top height variations. [For overhead sun, the escaping effects can still dominate the most heterogeneous scenes, which have very steep cloud sides (implying strong downward escape), and low cloud fractions (resulting in weak upward trapping)].

The four individual components of the horizontal transport effect can also be combined to examine whether the scene albedo is influenced more by those components that affect the transmission of downwelling photons (downward trapping and escape) than it is by those components that influence the emergence of upwelling photons from the cloud field (upward trapping and escape).

Figure 16 shows that the albedo is lowered mainly by making the transmission of downwelling photons easier for both extinction and cloud-top variations. This finding confirms previous studies (e.g., Cannon 1970; Davis 1992), which focused on downward escape as the main heterogeneity effect in clouds with internal extinction variability.

However, the figure also shows that for oblique sun, the situation reverses, and the effects that influence upwelling radiation become dominant. [The figure shows that the situation does not reverse for some scenes; however, the overall horizontal transport effect is very small (less than 0.0025) for all these scenes. Hence, the above conclusion is still valid for all scenes in which the albedo is affected significantly by horizontal transport.]

5. Effects on zenith reflectance

Numerous studies (e.g., Davies 1984; Bréon 1992; Kobayashi 1993) have shown that cloud heterogeneities affect not only the amount of radiation reflected but also its angular distribution. This section examines how heterogeneities affect cloud reflection in the direction most important to satellite remote sensing, toward the zenith (''zenith reflectance''). The reflectance, or bidirectional reflection factor (BRF), is defined as

$$\mathrm{BRF} = \frac{\pi I}{\mu_0 S_0},$$

where I is the reflected radiance, S_0 is the solar irradiance, and $\mu_0 = \cos\Theta_0$.

Loeb and Davies (1996b) used measurements of the Earth Radiation Budget Satellite Narrow Field of View broadband scanning radiometer to examine how zenith reflectance of real clouds varies with Θ_0. According to one-dimensional radiative transfer theory, zenith reflectance should decrease as Θ_0 increases. The reason for this decrease is that cloud particles scatter light predominantly in near-forward directions, and thus for large Θ_0, plane-parallel clouds tend to reflect the most radiation into oblique forward directions rather than in the zenith direction. However, when Loeb and Davies

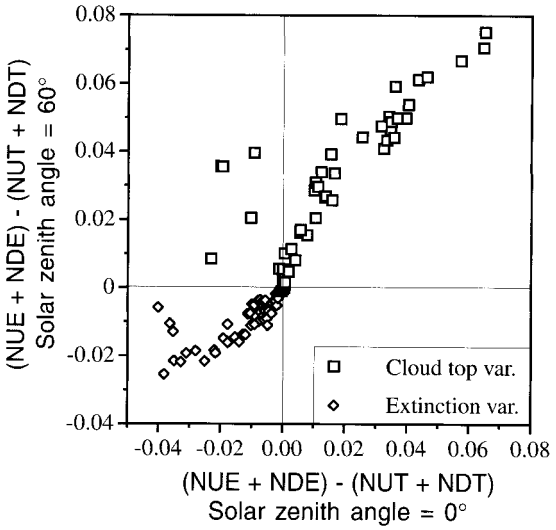

FIG. 15. Comparison of the effects of radiation flowing from thick to thin (NUE + NDE) and from thin to thick areas (NUT + NDT). Negative values indicate that the former flow has a larger effect; positive values, that the latter one decreases the scene albedo more. Acronyms as defined in Fig. 12.

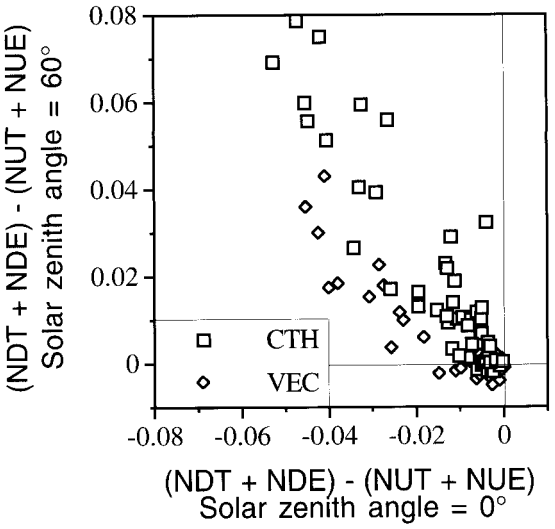

FIG. 16. Comparison of the influence that horizontal transport has on scene albedo by affecting transmission (NDT + NDE) and reflection (NUT + NUE). Negative values indicate that the albedo is decreased mainly by horizontal transport easing the transmission of radiation; positive values, that the albedo is decreased mainly by horizontal transport making cloud reflection more difficult. Acronyms as defined in Fig. 12.

(1996b) averaged all water clouds observed over the oceans between 30°N and 30°S, they found that zenith reflectance does not decrease but increases with Θ_0. Loeb and Coakley (1998) observed similar behavior in Advanced Very High Resolution Radiometer measurements of marine stratus clouds. Loeb et al. (1997) have suggested that this unexpected behavior may be due to cloud heterogeneities. This section examines whether cloud-top and/or extinction variations can cause such an increase, and if so, through what mechanisms. This question is addressed through the example of a cloud field generated using the same input parameters as in Loeb et al. (1997): CF = 0.75, $\langle\tau\rangle$ = 10, VEC = 30 km^{-1}, $s_{(k)} = 1$ if $k \leq 6$, and $s_{(k)} = 3.6$ if $k > 6$. (Since the generation process uses some random numbers that are different in the two studies, using the same input parameters does not result in identical, only in statistically similar, cloud fields.)

The results shown in Fig. 17 indicate that zenith reflectance increases sharply with Θ_0 for cloud-top variations, increases much less for extinction variations, and, as expected, decreases for homogeneous clouds. One reason for the differences is that as Θ_0 increases, heterogeneous clouds intercept more and more solar radiation (through their sides) thus increasing the amount of radiation that is potentially available for zenith reflection. Figure 18 shows that when μ_0 decreases from 1 to 0.15, this effect (calculated using TIPA) is responsible for about 15% and 20% of the zenith reflectance's deviation from that of a single homogeneous cloud layer for cloud-top and extinction variations, respectively. The rest of the differences are due to changes in the horizontal transport effect, especially a large increase in upward trapping and a smaller increase in downward trapping (Fig. 19). Both these effects scatter radiation after it would have already left a plane-parallel cloud; they reduce the radiation that goes in the forward direction, and distribute it in all directions, thereby increasing zenith reflectance. (For oblique sun, upward trapping affects zenith reflectance and albedo in opposite ways: it enhances the former, while it decreases the latter, predominantly by reducing reflection in the forward direction.) Section 4 discusses the reasons these

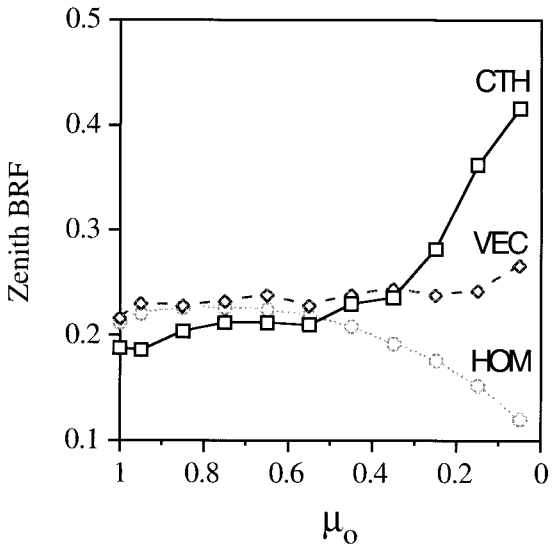

FIG. 17. Zenith reflectance (BRF) as a function of μ_0 for scenes with cloud-top (solid line) and extinction variations (dashed line) and for a scene that contains a homogeneous cloud (dotted line).

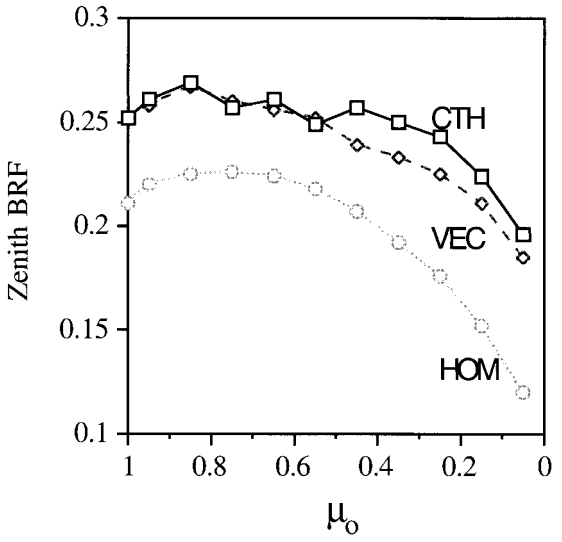

FIG. 18. Zenith reflectance for the same scenes as in Fig. 17 but calculated using TIPA instead of three-dimensional Monte Carlo simulations.

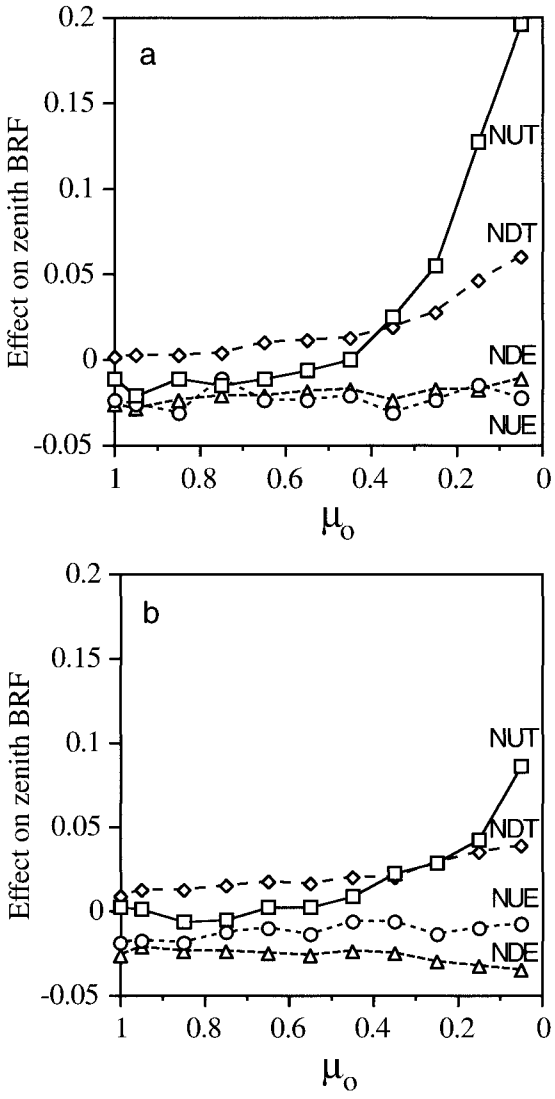

FIG. 19. Influence of each component of the horizontal transport effect on zenith reflectance: (a) cloud-top variations and (b) extinction variations. Acronyms as defined in Fig. 12.

two effects increase more for cloud-top than for extinction variations, whereas the other two effects (upward and downward escape) remain fairly constant.

Downward trapping and the sum of upward and downward escapes both change fairly similarly for cloud-top and extinction variability. As described in section 4, however, upward trapping increases much more for cloud-top than for extinction variations. Therefore, one can say that for this cloud field, downward trapping and the one-dimensional heterogeneity effect counterbalance the decrease in zenith reflectance expected for homogeneous clouds, while changes in upward trapping cause the various increases obtained for the two heterogeneity types.

Comparison of Figs. 17 and 4 of Loeb and Davies (1996b) could suggest that the observed behavior in zenith cloud reflection is most similar to the behavior of clouds with extinction variability. However, since the observational results include many measurements of relatively homogeneous cloud scenes, the decrease for these homogeneous scenes must be counteracted by a strong increase for the heterogeneous scenes. Thus, it appears more likely that cloud-top, rather than extinction, variations are responsible for the behavior observed by Loeb and Davies (1996b).

6. Summary and conclusions

Although earlier studies introduced such terms as channeling, plane-parallel albedo bias, and side illumination to explain specific aspects of the radiative heterogeneity effects, it has been difficult to apply these terms to more general types of heterogeneity. The main goal of the present study has been to extend these earlier studies by presenting a more general approach to the explanation of heterogeneity effects.

Instead of examining how heterogeneities change radiance and flux values at various fixed locations, as in earlier approaches, this paper considers how individual photons are influenced by heterogeneities as they move along their paths within the cloud layer. The difference between the present approach and previous ones is analogous to the difference between the Lagrangian and Eulerian approaches used, for example, in fluid dynamics.

Using the adopted approach, this study established a theoretical framework, which defines and evaluates the various mechanisms through which cloud heterogeneities influence solar radiation. The main advantages of the proposed framework are as follows.

- It reflects the physical processes through which cloud heterogeneities influence shortwave radiation.
- It is based on unambiguous, quantitative definitions that are easy to calculate.
- It uses measures of the effects of heterogeneity that complement each other without overlap; that is, they can simply be added up to obtain the overall heterogeneity effect.
- It can be used for any irregular cloud field. All heterogeneities—for example, internal volume extinction coefficient variations and the effects of cloud brokenness—can be handled within a unified framework.

The proposed system is based on the understanding that the single most important factor influencing a cloud field's radiative properties is the amount of various scattering and absorbing substances, and that this amount can be used to obtain first-order estimates for the field's radiative properties through the assumption of a homogeneous spatial distribution of all scattering and absorbing substances. Thus, this paper defined the radiative heterogeneity effect as the difference between the radiative transfer result for the true three-dimensional cloud field and the result obtained if the same amount of scatterers and absorbers were distributed homogeneously throughout the entire volume of the scene.

To explain the fairly complex radiative effect of cloud heterogeneity, the proposed framework divides the effect into two main components: the one-dimensional heterogeneity effect and the horizontal transport effect. The one-dimensional heterogeneity effect addresses the fact that photons enter the cloud layer at regions of various optical properties, and the horizontal transport effect considers the additional consequences that arise when multiple scattering takes these photons to other regions, where they encounter cloud properties different from those at their points of entry.

To calculate the magnitude of the first component, the study has developed a one-dimensional radiative transfer approximation called the tilted independent pixel approximation (TIPA). An important advantage of the TIPA is that, unlike the widely used independent pixel approximation (IPA), it uses the horizontal distribution of the slant optical thickness with respect to the direct solar beam. This allows TIPA to explain various phenomena that cannot be explained using IPA; for example, that cloud streets parallel and perpendicular to the sun have different radiative properties. In addition, TIPA tends to give more accurate albedo estimates than IPA for solar zenith angles greater than 50°–60°. Finally, TIPA also gives more accurate results than IPA for cases of strong absorption since it always reduces to the correct answer for direct beam transmission as the single-scatter albedo tends to zero.

However, results also indicate that even if the TIPA is used, a one-dimensional framework is not sufficient to fully describe numerous phenomena since horizontal transport is often also very important. This study identified four mechanisms through which horizontal transport influences solar radiation: upward trapping, downward trapping, upward escape, and downward escape. A procedure to calculate the amount of radiation affected by these four mechanisms, and to obtain their net effects from Monte Carlo simulations, was also presented.

The proposed framework was then used to quantitatively examine various aspects of the heterogeneity effects that occur in irregular cloud fields. It was found that identical variations in cloud optical thickness can cause much stronger heterogeneity effects if they are due to variations in cloud-top height (i.e., in geometrical cloud thickness) rather than in the volume extinction coefficient (assuming flat cloud tops), as assumed in most previous studies of irregular cloud fields. For overhead sun, the differences in albedo are comparable in magnitude to the horizontal transport effects themselves and can exceed 0.05. For oblique sun, the differences are smaller but can still be significant.

The differences between the flat and variable cloud-top effects were explained by examining the individual components of the overall heterogeneity effect. For extinction variations, downward escape is the strongest component of the horizontal transport effect, whereas for cloud-top variations, its other three components can be at least as important. Combining the individual components of the horizontal transport effect revealed that, as suggested in previous studies, the main means by which this effect decreases the albedo of clouds with extinction variations is the transport of radiation from thick to thin regions. In case of cloud-top variations, however, the main means is the horizontal transport of radiation from thin to thick regions. It was also found that for oblique sun, the horizontal transport effect decreases the scene albedo primarily by making the reflection of upwelling radiation within the cloud more difficult. This finding was somewhat unexpected since previous studies focused more on horizontal transport decreasing the scene albedo by making the transmission of downwelling radiation easier.

As expected, horizontal transport was found to decrease the albedo of all scenes having extinction variations. However, it was found that for overhead sun, the horizontal transport effect due to cloud-top variations can increase the albedo for some clouds even if neither absorption nor surface reflection is present. The increase (which was less than 0.01 for all cases) occurs for scenes with slightly sloped cloud sides and large cloud fractions and is due to a relatively strong upward escape effect. Although horizontal transport still decreased the albedo of most scenes with cloud-top variations, the above result implies that IPA underestimates the albedo of some heterogeneous cloud scenes even for overhead sun.

This study also investigated how heterogeneities affect cloud reflection toward the zenith, a direction that is especially important for satellite remote sensing. In particular, it explained why clouds reflect a relatively

larger portion of the incoming solar radiation toward the zenith for oblique than for overhead sun (Loeb and Davies 1996b; Loeb and Coakley 1998). This phenomenon is opposite to the behavior of homogeneous clouds, which have flat tops, and Loeb et al. (1997) have suggested that it may be due to the effect of cloud heterogeneities, especially cloud-top variations. The present study explained that this is because the heterogeneities make it more difficult for radiation to leave the cloud in oblique forward directions. The results indicate that the relative difference between the scene average zenith reflectance of cloud fields with cloud-top and extinction variations can exceed 25% for overhead sun and 50% for oblique sun.

Overall, this paper can be summarized in the following main points. First, it proposed a new theoretical framework to examine the radiative effects of cloud heterogeneities and provided an example to demonstrate how this framework can be used. Second, it showed that the radiative properties of cloud fields with significant cloud-top variations may be quite different from the properties suggested in previous studies, which either used simple cloud geometries, such as cubes, or attributed all optical thickness variations to changes in the VEC and kept the geometrical cloud thickness constant. Third, it offered new insights into how radiative heterogeneity effects work.

We believe that the new concepts introduced in this paper can also be useful in future studies. Examples of possible future applications include the following.

- TIPA may be used for quick radiative transfer calculations.
- While the present study focused entirely on cloud reflection, future studies analyzing cloud absorption, transmission, or actinic fluxes may also find it useful to adapt the approach presented here: to follow the path of individual photons in order to see how cloud heterogeneities influence them, instead of considering only how heterogeneities influence the radiation field at fixed locations. The proposed description of heterogeneity effects may also offer new insights in studies that examine the effects of vertical heterogeneity and the three-dimensional distribution of cloud microphysical properties.
- The proposed theoretical framework and definitions of heterogeneity effects can also be useful in parameterizing the radiative effects of cloud heterogeneities. Since the overall heterogeneity effect is a combination of individual mechanisms that depend on different cloud parameters (e.g., magnitude of cloud variability at different scales), it may be easier to first parameterize these mechanisms individually and then combine their results rather than parameterizing the complex overall effects in one step.
- The new insights into how cloud-top variations and extinction variations affect solar radiation may be helpful in explaining future observations of heterogeneous cloud scenes.

The results presented here are based on heterogeneous cloud fields that cover a wide range of cloud properties and are consistent with satellite observations. While we expect the qualitative findings to be applicable to other types of cloud fields as well, additional studies based on a climatologically more representative variety of cloud types would be of interest in further examining the presented hypotheses.

Acknowledgments. Funding for this research from the Jet Propulsion Laboratory of the California Institute of Technology under Contract 959085 is gratefully acknowledged. The authors wish to thank Larry Di Girolamo and Laura Atwood for proofreading the manuscript and providing many helpful suggestions, and Bruce Wielicki for making the examined Landsat images available for this study. This paper is based on the Ph.D. dissertation of Tamás Várnai.

REFERENCES

Aida, M., 1977: Reflection of solar radiation from an array of cumuli. *J. Meteor. Soc. Japan,* **55,** 174–181.

Barker, H. W., 1994: Solar radiative transfer for wind-sheared cumulus cloud fields. *J. Atmos. Sci.,* **51,** 1141–1156.

——, and J. A. Davies, 1992a: Solar radiative fluxes for stochastic, scale-invariant broken cloud fields. *J. Atmos. Sci.,* **49,** 1115–1126.

——, and ——, 1992b: Cumulus cloud radiative properties and the characteristic of satellite radiance wavenumber spectra. *Remote. Sens. Environ.,* **42,** 51–64.

Boers, R., J. D. Spinhirne, and W. D. Hart, 1988: Lidar observations of the fine-scale variability of marine stratocumulus clouds. *J. Appl. Meteor.,* **27,** 797–810.

Bréon, F.-M., 1992: Reflectance of broken cloud fields: Simulation and parameterization. *J. Atmos. Sci.,* **49,** 1221–1232.

Busygin, V. P., N. A. Yevstratov, and Ye. M. Feygelson, 1973: Optical properties of cumulus clouds, and radiative fluxes for cumulus cloud cover. *Izv. Acad. Sci. USSR, Atmos. Oceanic Phys.,* **9,** 648–653.

Cahalan, R. F., 1989: Overview of fractal clouds. *Advances in Remote Sensing Retrieval Methods,* H. E. Fleming and J. S. Theon, Eds., Deepak Publishing, 371–389.

——, and J. B. Snider, 1989: Marine stratocumulus structure. *Remote Sens. Environ.,* **28,** 95–107.

——, W. Ridgway, W. Wiscombe, T. L. Bell, and J. B. Snider, 1994: The albedo of fractal stratocumulus clouds. *J. Atmos. Sci.,* **51,** 2434–2455.

——, D. Silberstein, and J. B. Snider, 1995: Liquid water path and plane-parallel albedo bias during ASTEX. *J. Atmos. Sci.,* **52,** 3002–3012.

Cannon, J. C., 1970: Line transfer in two dimensions. *Astrophys. J.,* **161,** 255–264.

Chambers, L. H., B. A. Wielicki, and K. F. Evans, 1997: Accuracy of the independent pixel approximation for satellite estimates of oceanic boundary layer cloud optical depth. *J. Geophys. Res.,* **102,** 1779–1794.

Davies, R., 1976: The three-dimensional transfer of solar radiation in clouds. Ph.D. thesis, University of Wisconsin—Madison, 220 pp. [Available from Memorial Library, University of Wisconsin—Madison, 728 State St., Madison, WI 53706.]

——, 1978: The effect of finite geometry on the three-dimensional

transfer of solar irradiance in clouds. *J. Atmos. Sci.,* **35,** 1712–1725.

——, 1984: Reflected solar radiances from broken cloud scenes and the interpretation of scanner measurements. *J. Geophys. Res.,* **89,** 1259–1266.

——, W. L. Ridgway, and K.-E. Kim, 1984: Spectral absorption of solar radiation in cloudy atmospheres: A 20 cm^{-1} model. *J. Atmos. Sci.,* **13,** 2126–2137.

Davis, A., 1992: Radiation transport in scale invariant media. Ph.D. thesis, McGill University, 325 pp. [Available from PSE Library, McGill University, 809 Sherbrooke St. West, Montreal, PQ H3A 2K6, Canada.]

——, A, Marshak, R. Cahalan, and W. Wiscombe, 1997: The Landsat scale break in stratocumulus as a three-dimensional radiative transfer effect: Implications for cloud remote sensing. *J. Atmos. Sci.,* **54,** 241–260.

Duda, D. P., G. L. Stephens, B. Stevens, and W. R. Cotton, 1996: Effects of aerosol and horizontal inhomogeneity on the broadband albedo of marine stratus: Numerical simulations. *J. Atmos. Sci.,* **53,** 3757–3769.

Gabriel, P. M., and K. F. Evans, 1996: Radiative transfer methods for calculating domain-averaged solar fluxes in inhomogeneous clouds. *J. Atmos. Sci.,* **53,** 858–877.

Hayasaka, T., N. Kikuchi, and M. Tanaka, 1995: Absorption of solar radiation by stratocumulus clouds: Aircraft measurements and theoretical calculations. *J. Appl. Meteor.,* **34,** 1047–1055.

Hignett, P., and J. P. Taylor, 1996: The radiative properties of inhomogeneous boundary layer cloud: Observations and modelling. *Quart. J. Roy. Meteor. Soc.,* **122,** 1341–1364.

Kobayashi, T., 1988: Parameterization of reflectivity for broken cloud fields. *J. Atmos. Sci.,* **45,** 3034–3045.

——, 1993: Effects due to cloud geometry on biases in the cloud albedo derived from radiance measurements. *J. Climate,* **6,** 120–128.

Loeb, N. G., and R. Davies, 1996a: Angular dependence of observed radiation field: A comparison with plane-parallel theory. *J. Geophys. Res.,* **102,** 6865–6881

——, and ——, 1996b: Observational evidence of plane-parallel model biases at low sun elevations. *J. Geophys. Res.,* **101,** 1621–1634.

——, and J. A. Coakley Jr., 1998: Inference of marine stratus cloud optical depths from satellite measurements: Does 1D theory apply? *J. Climate,* **11,** 215–233.

——, T. Várnai, and R. Davies, 1997: Solar zenith angle dependence of solar radiation reflected from inhomogeneous clouds. *J. Geophys. Res.,* **102,** 9387–9395.

——, T. Várnai, and D. M. Winker, 1998: Influence of sub-pixel scale cloud-top structure on reflectances from overcast stratiform cloud layers. *J. Atmos. Sci.,* **55,** 2960–2973.

Marshak, A., A. Davis, W. Wiscombe, and R. Cahalan, 1995a: Radiative smoothing in fractal clouds. *J. Geophys. Res.,* **100,** 26 247–26 261.

——, ——, ——, and G. Titov, 1995b: The verisimilitude of the independent pixel approximation used in cloud remote sensing. *Remote Sens. Environ.,* **52,** 71–78.

——, ——, R. F. Cahalan, and W. Wiscombe, 1998: Nonlocal independent pixel approximation: Direct and inverse problems. *IEEE Trans. Geosci. Remote Sens.,* **36,** 192–205.

McKee, T. B., and S. K. Cox, 1974: Scattering of visible radiation by finite clouds. *J. Atmos. Sci.,* **31,** 1885–1892.

Minnis, P., 1989: Viewing zenith angle dependence of cloudiness determined from coincident GOES east and west data. *J. Geophys. Res.,* **94,** 2303–2320.

Newman, W. I., J. K. Lew, G. L. Siscoe, and R. G. Fovell, 1995: Systematic effects of randomness in radiative transfer. *J. Atmos. Sci.,* **52,** 427–435.

Oreopoulos, L., 1996: Plane-parallel albedo bias from satellite measurements. Ph.D. thesis, McGill University, 142 pp. [Available from PSE Library, McGill University, 809 Sherbrooke St. West, Montreal, PQ H3A 2K6, Canada.]

——, and R. Davies, 1998: Plane-parallel albedo biases from satellite observations. Part I: Dependence on resolution and other factors. *J. Climate,* **11,** 919–932.

Snow, J. W., J. Bunting, R. d'Entremont, D. Grantham, K. Hardy, and E. Tomlinson, 1985: Space shuttle cloud photographs assist in correcting meteorological satellite data. *Eos, Trans. Amer. Geophys. Union,* **66,** 489–490.

Tessier, Y., S. Lovejoy, and D. Schertzer, 1993: Universal multifractals: Theory and observation for rain and clouds. *J. Appl. Meteor.,* **32,** 223–250.

Várnai, T., 1996: Reflection of solar radiation by inhomogeneous clouds. Ph.D. thesis, McGill University, 149 pp. [Available from PSE Library, McGill University, 809 Sherbrooke St. West, Montreal, PQ H3A 2K6, Canada.]

Welch, R. M., and B. A. Wielicki, 1984: Stratocumulus cloud field reflected fluxes: The effect of cloud shape. *J. Atmos. Sci.,* **41,** 3085–3102.

——, S. K. Cox, and J. M. Davis, 1980: *Solar Radiation and Clouds. Meteor. Monogr.,* No. 39, Amer. Meteor. Soc., 96 pp.

Wendling, P., 1977: Albedo and reflected radiance of horizontally inhomogeneous clouds. *J. Atmos. Sci.,* **34,** 642–650.

Zuidema, P., and K. F. Evans, 1998: On the validity of the independent pixel approximation for boundary layer clouds observed during ASTEX. *J. Geophys. Res.,* **103,** 6059–6074.